machines

MDPI

Article

Experimental Validation and Dynamic Analysis of Additive Manufacturing Burner for Gas Turbine Applications

Alessio Cascino [1,*], Enrico Meli [1], Andrea Rindi [1], Egidio Pucci [2] and Emanuele Matoni [2]

[1] Department of Industrial Engineering, University of Florence, 50139 Florence, Italy; enrico.meli@unifi.it (E.M.); andrea.rindi@unifi.it (A.R.)
[2] Baker Hughes, Nuovo Pignone Tecnologie, 50127 Florence, Italy; egidio.pucci@bakerhughes.com (E.P.); emanuele.matoni@bakerhughes.com (E.M.)
* Correspondence: alessio.cascino@unifi.it

Abstract

In the context of a rapidly evolving energy sector, the development of hydrogen-ready gas turbines, a key milestone in the energy transition toward decarbonization, requires advanced gas injectors capable of operating with both natural gas and hydrogen. Additive manufacturing (AM) significantly accelerates the iterative design process, enabling the production of single-piece, fully three-dimensional components and supporting rapid prototyping with optimized process parameters. Early assessment of component durability, particularly structural damping, is crucial to predicting dynamic response and high-cycle fatigue life, reducing costly design modifications in later stages. In this work, a methodology is proposed for structural damping characterization at the early prototypal stage, combining ping test measurements with a numerical approach based on the Half-Power Bandwidth Method (HBM) enhanced by an iterative procedure. This approach enables the accurate estimation of representative damping values for low-mass, high-stiffness components, overcoming the limited accuracy of standard Rayleigh damping models at this stage. The methodology was applied to a gas turbine burner manufactured via additive manufacturing, demonstrating that even with partial experimental data, it is possible to obtain reliable damping estimates, support rapid design iteration, and ensure convergence toward optimal mechanical performance.

Keywords: gas turbine; hydrogen; additive manufacturing; dynamic verification; modal analysis; ping test; damping ratio; fuel burner; gas injector; 3D printing

check for updates

Academic Editors: Panagiotis Kyratsis and Alexios Papacharalampopoulos

Received: 20 October 2025
Revised: 21 November 2025
Accepted: 27 November 2025
Published: 1 December 2025

Citation: Cascino, A.; Meli, E.; Rindi, A.; Pucci, E.; Matoni, E. Experimental Validation and Dynamic Analysis of Additive Manufacturing Burner for Gas Turbine Applications. *Machines* **2025**, *13*, 1111. https://doi.org/10.3390/machines13121111

Copyright: © 2025 by the authors. Licensee MDPI, Basel, Switzerland. This article is an open access article distributed under the terms and conditions of the Creative Commons Attribution (CC BY) license (https://creativecommons.org/licenses/by/4.0/).

1. Introduction

Natural gas-powered plants could play a significant role in the CO_2-free electricity production and for the grid stabilization needs to meet the decarbonization objectives in the energy production sector, which have been designed to limit the negative effects of climate change. Gas turbine assets are the core part of the decarbonization effort in the power plant, since they offer the possibility of using existing infrastructure with their well-proven flexibility, changing the burned fuel composition to one that is free of carbon fuels. Hydrogen, as fuel, is an essential pillar of CO_2-free, dispatchable power generation: the ability for existing gas turbine peaker units to operate on hydrogen-based fuels is a key future requirement to fulfill the target of CO_2-free power generation, allowing the energy producers to substantially reduce or even eliminate carbon emissions, guaranteeing supply continuity, offering the same grid ancillary services and avoiding stranded assets,

whilst ensuring protection of power generation investments. The EU strategy currently aims to achieve carbon-free energy markets by 2050, which implies that Europe's inventory of fossil power plants will gradually be replaced with renewable energy resources [1–4]. In this transition, as the renewables share increases, the need for balancing power will increase significantly, and the system will be challenged to the limits of what current carbon-free systems can achieve. The integration of hydrogen in an existing gas power plant is a complex endeavor with direct impact on auxiliaries, the fuel supply system, plant operation and safety. Gas turbine combustors, typically designed and operated with traditional fuels like natural gas and diesel oils, shall then be redesigned to extend the ability of burning carbon-free fuels, like hydrogen or ammonia [5,6]. To achieve the hydrogen-burning ability, one of the most impacted components of the gas turbine is the fuel injector, or burner, which shall include new technologies in the design, such as flashback resistance and the fully premixing of fuel and oxidant flows [7–16]. In addition to the technology requirements related to the functional performance of the gas injector, which typically constrains the size, number and position of gas injection holes and the fuel and air paths, there is also a product requirement regarding the sealing of the fuel gas paths: hydrogen is indeed the smallest molecule, and the sealed joints designed to work with natural gas could not guarantee the desired minimum leak rate. Combined with the high reactivity and the wide range of flammability of hydrogen in air, eventual leaks need to be detected and vented opportunely to avoid any risk of deflagration, or even detonation, inside the gas turbine enclosure [17]. Additive manufacturing is the one of the most effective technologies to address the issue of the hydrogen leaks: single-piece burners can be printed without the need for internal sealing joints, even with complex tridimensional geometries of fuel and air paths, minimizing the eventual sources of external leaks for the fuel gas system. Among the technological challenges related to the development of gas turbine combustion systems suitable for hydrogen combustion, materials and coating characterization in a rich hydrogen environment is one of the most expensive in terms of time and budget. The hydrogen embrittlement is introducing a degradation effect on the mechanical characteristics of the materials exposed to a partial pressure of hydrogen, reducing the durability of the components: To enable a robust evaluation of the expected service life of the components against the product requirements for mean time between maintenance, verification tests on the material properties shall be carried out. In recent years, numerous examples can be found regarding applications of Metal Additive Manufacturing in the production of turbomachinery and aerospace components. In [18,19], some of the main techniques used in this field are described. One of the most widely used groups of techniques is Powder Bed Fusion (PBF) [20]. This group includes Laser Powder Bed Fusion (L-PBF), which uses high-power lasers for the local melting of metal powders, and Electron Beam Powder Bed Fusion (EB-PBF), which uses a high energy electron beam instead. Another widely used group of Metal AM techniques is the one based on Directed Energy Deposition (DED) [21]. In this case, there is no powder bed, and the layer of molten material is fed through a wire feedstock. The increase in production through AM techniques has been made possible by the development of new materials [22]. Many alloys have been applied to this emerging technology such as custom aluminum alloys, titanium alloys, nickel- and iron-based superalloys, copper alloys, cobalt alloys, refractory alloys and steels. Metal Additive Manufacturing has proven to be suitable for building many different components for gas turbine and compressors [23–29] and in particular for gas turbine fuel nozzles, heat exchangers, heat sinks, heat pipes and others [30]. The primary advantage has been proven to be the ability of this technology to realize complex internal geometries [31]. The use of additive manufacturing as a production process may introduce some unknowns regarding the behavior and properties of materials. In particular, the dynamic behavior of

the component in question may not exactly replicate that of an equivalent one produced with traditional techniques such as casting or similar. The research work presented in [32] investigates how dynamic mechanical properties of AM components can be affected by several important 3D printing parameters, including layer thickness and orientation, post-processing techniques, the density of infill and patterns, and the material microstructure. Typically, in the design phase of innovative components, and in particular the fuel nozzles, the structural damping is verified by dynamic measurements of produced parts, eventually requiring design changes if impacting the component operational lifespan. The integration of the structural damping prediction in the early phases of the design process with the AM technology and material peculiarities is fundamental to reduce the time to market and cost of the development of new components.

2. Materials and Methods

2.1. Burner Design for Additive Manufacturing

The difficulty of reaching ever more stringent emission values grows hand in hand with the increase in the complexity of the geometry of the components and, in particular, of the fuel burners. The adoption of additive manufacturing (AM) allows to overcome the typical constraints of the traditional manufacturing techniques even when introducing a different set of process constraints that is unusual for this manufacturing technology. AM technology, if used in conjunction with traditional technology, can provide added value not only for prototyping but also for production [33]. Including a brief consideration about gas turbine efficiency and overall energy efficiency, these performance aspects are closely linked to the improved manufacturability and design flexibility enabled by AM. In particular, the geometric freedom offered by AM facilitates the production of optimized cooling channels, lightweight structures, and complex aerodynamic features, which can substantially enhance thermal efficiency and thus contribute to higher overall energy performance in gas turbine systems. One of the advantages of building a fuel burner by AM is that considering the design rules, it is possible to print the parts as a single piece reducing the production lead time and supply chain and, primarily, avoid any sealing system on the connections between the parts of the system. Typically, during the first phase of the project, different designs of fuel burners are tested on a single burner test bench to verify the component functional requirements and, comparing test results, define the best design to be tested on a functionally representative combustion system. To minimize the procurement of the parts to be tested, AM technology is used from the earliest phases of the projects as rapid prototyping technology, realizing some component trials to define the correct reshaping of functional features and to compensate for the shrinkage or deformation of the parts. An AM technique featuring metal powders was employed, enabling the fabrication of components with complex geometries, as well as air and gas channels featuring variable cross-sections and three-dimensional paths, while also respecting the particular technology limits such as the maximum angle with respect to the direction of material deposition, the minimum wall thickness, the minimum width for slots or plenum, and the minimum diameter for injection holes [34]. All such features play an important role in the complete evacuation of the powder from the internal cavities and channels after the printing: the complexity of the powder removal process is proportional to the geometrical complexity of the parts. A significant aspect to be considered during the design development phase is the measurability of the printed parts as a single piece. Design with complex geometries cannot be measured directly with standard measurement tools and could require the designer to introduce some specific design features to allow the measurement of functional parameters. Passing from a fuel burner composed of many parts produced by a traditional manufacturing process to a single piece fuel burner made by AM, the ability to measure

features of interest with standard methods in a disassembled condition could be lost. The same features, in a single piece part, could not be accessible for standard measurement tools, and alternative measurement methods, such as flow tests or computer tomography, need to be validated during trialing and qualification phases. As for all welding processes, to increase the durability of the parts and in some cases allow the complete printing of the parts, it is important to implement the design rules to reduce the residual stresses. A well-suited AM design is the most effective solution to avoid residual stresses after printing: the design guidelines are the same as those typically used for injection molding and casting manufacturing methods. A post-printing stress relief heat treatment is recommended. AM technology introduction is impacting also the approach used for component durability assessment: durability assessment of the printed parts requires knowing the eventual residual stresses that result from the production process, the material properties, including the structural damping analyzed in the next sections of this work, and, in case of hydrogen applications, if the material is affected by hydrogen embrittlement. In the prototypal production phase, additional specimens could be printed during components production in order to perform material characteristics tests in a hydrogen environment and evaluate the effects of embrittlement on the durability of the parts.

2.2. Methodology

In this section, the methodology adopted for the dynamic verification of a gas turbine burner produced by additive manufacturing is presented. The approach combines numerical and experimental techniques to estimate modal damping with the objective of providing a reliable and efficient assessment in the early stage of component development. The methodology exploits a digital twin of the burner, validated through an experimental ping test, to extract modal properties and damping estimates in a representative frequency range of interest. Starting from the CAD model of the burner, a finite element (FE) model was developed. Modal analysis was carried out to identify the natural frequencies and mode shapes of the system, simulating both free-free and constrained configurations. The free-free case was considered to evaluate the intrinsic dynamic characteristics of the component without the influence of external boundaries, while the constrained configuration reproduced the operational condition in which the burner is mounted on the engine structure. This dual analysis provided a comprehensive framework for planning the experimental activity, including the definition of excitation and response points. The experimental activity was based on an instrumented ping test, which was selected for its ability to provide a rapid, cost-effective, and reliable characterization of modal parameters. Despite its impulsive nature, which typically results in small vibration amplitudes, the ping test was considered well suited to the present study because the main objective was not to replicate full-service loading conditions but rather to establish a robust numerical–experimental correlation in the prototyping phase. Moreover, the technique allowed a precise identification of natural frequencies and mode shapes, which are crucial for validating the digital twin. The Modal Assurance Criterion (MAC) was used to quantify the correlation between numerical and experimental mode shapes. Once validated, the FE model was employed to replicate the ping test conditions and compare the numerical and experimental frequency response functions. This comparison enabled the estimation of structural damping through the Half-Power Bandwidth Method (HBM), which is a well-established technique for deriving damping ratios from response spectra. The method provided stable and consistent results, confirming its suitability for early-stage dynamic characterization. In modeling the burner assembly, the connection zones ensured a realistic representation of boundary conditions while maintaining a level of simplicity consistent with the prototyping phase. It is recognized that a more detailed modeling of the bolted

interfaces, including nonlinear contact effects and friction coefficients, could improve the prediction of amplitude-dependent damping. However, this level of refinement is more appropriate for subsequent design phases once the component has been validated at a global level. Although nonlinearities may arise in systems with complex geometries and materials, such as those produced by additive manufacturing, the present methodology focused on a linear modal characterization. The importance of considering nonlinear effects is acknowledged, and their inclusion will be relevant in future developments to improve prediction accuracy under operational loading conditions [35–40]. In summary, the proposed methodology combines numerical simulation and experimental validation into a coherent framework that is fast, efficient, and sufficiently accurate for early-stage design. The use of the digital twin, validated by ping test data, enables reliable damping estimation while minimizing experimental costs and time. This approach is particularly advantageous when dealing with innovative geometries manufactured through additive processes, where rapid feedback on dynamic behavior is essential to guide further design and testing activities.

2.3. Structural Dynamics Verification of AM Burner

2.3.1. Finite Element Model

The burner is composed of 13 components, including seals and connectors. These components presented a neglected mass with respect to the other ones and consequently do not have any effect in terms of global dynamic behavior. Then, they were suppressed from the model, maintaining only 4 components, as shown in Figure 1.

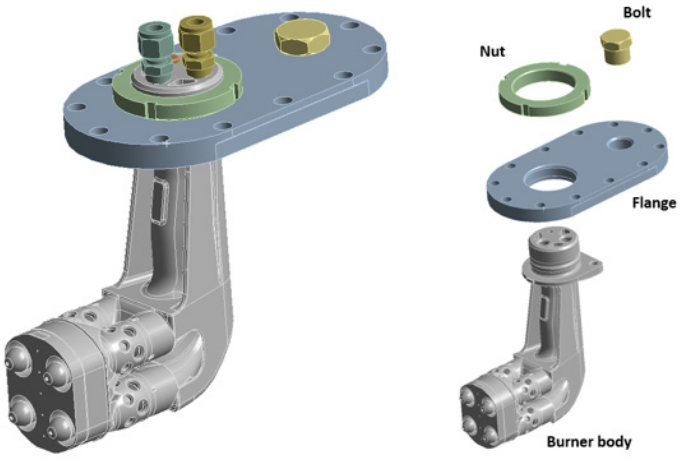


Figure 1. Main components of AM burner.

After careful cleaning and preparation of the geometries, a high-quality mesh was generated to ensure accurate numerical results. The cleaning process required particular attention due to the complex geometry of the burner, which includes thin walls, internal cavities, and intricate features that could negatively affect the mesh quality if not properly addressed. Only second-order tetrahedral elements (Tetra 10) were used, providing reliable stiffness evaluation and capturing the geometric details of the model. The final mesh consisted of 368,428 elements and 640,385 nodes. Four bonded contact interfaces were included, ensuring zero relative motion and maintaining the original gap between contacting surfaces. This setup enabled the model to accurately capture the structural response of the burner body. Regarding the materials, the assembly consisted of three types of structural steel and one of a super nickel alloy. The FE model is shown in Figure 2, where the red arrow indicates the flange face where the constrained condition is applied, simulating the assembly to the vessel of the combustion chamber.

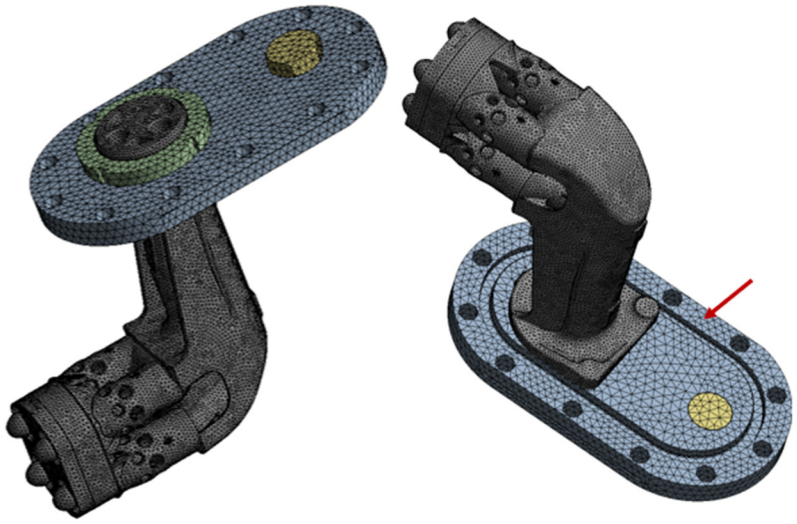


Figure 2. Finite element model of AM burner.

2.3.2. Numerical Pre-Test

Modal analysis has been carried out both for free-free and constrained configurations to define the suitable conditions for the next experimental test. The reference frequency range considered in the analysis spanned from 0 to 3000 Hz. The output of this analysis was the natural eigenvalues and eigenvectors of the burner assembly, which were required for the definition of the minimum set of measurement and excitation points to be used during the ping test. The use of the natural eigenvalues and eigenvectors also allows us to highlight, as clearly as possible, all the modes shapes found with the numerical modal analysis. The measurement points wireframe is shown in Figure 3.

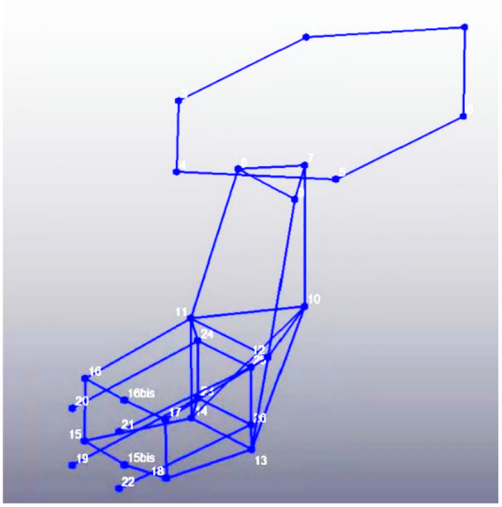


Figure 3. Measurement points wireframe.

2.3.3. Experimental Ping Test Setup

The experimental setup aimed to estimate the most important quantities to characterize the dynamic behavior of the system: frequencies of vibration, mode shapes and harmonic response. This last one includes the frequency response functions and the experimental modal damping ratio associated to each mode of the system in the free-free and constrained configurations. For free-free configuration, the burner has been suspended using an elastic cord attached to a crane, while in the constrained configuration, the burner has been

fastened to a combustor vessel. Refer to Figure 4a,b for visual representations of these distinct test conditions.

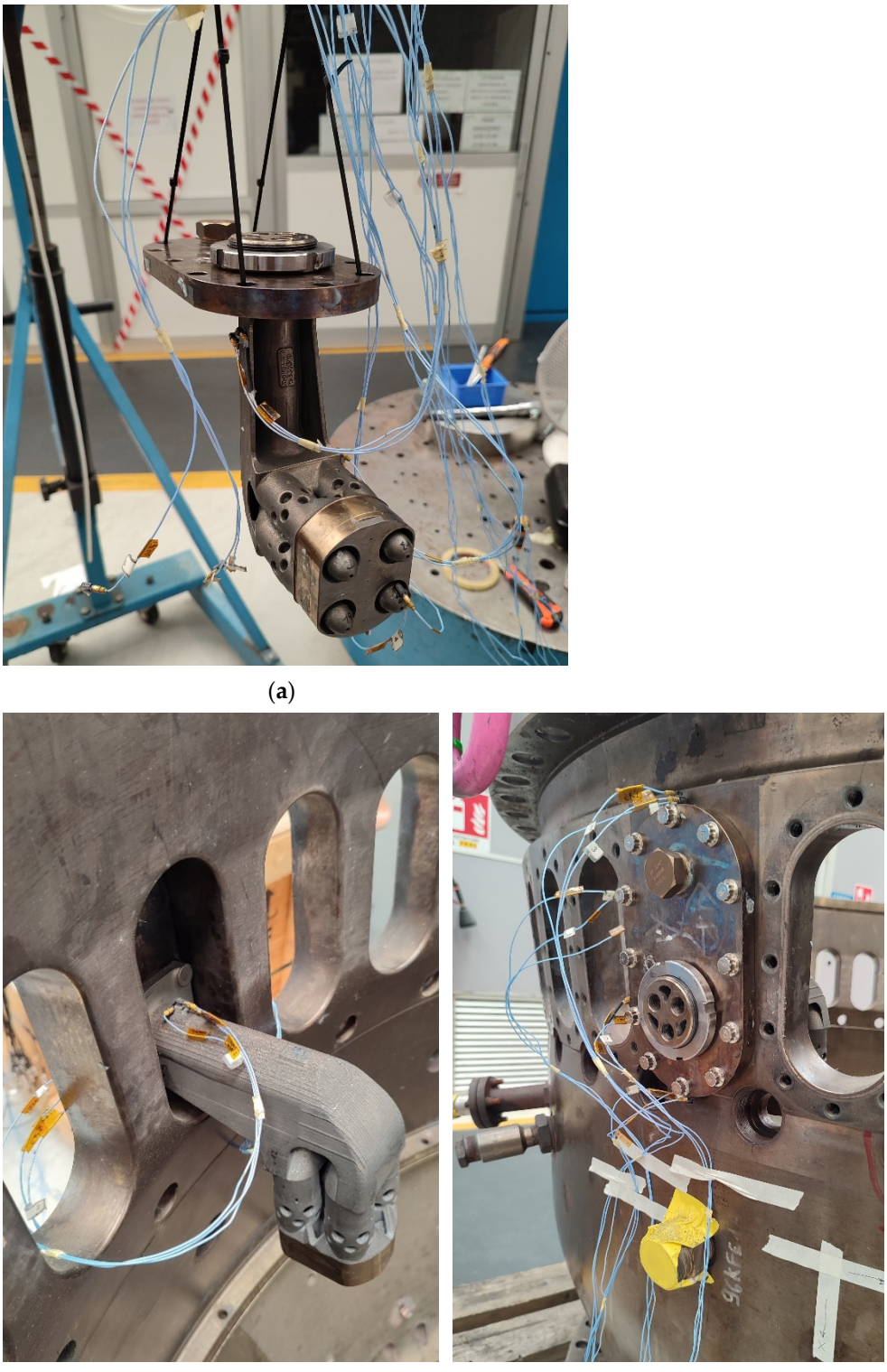


Figure 4. Experimental test configurations: (**a**) free-free, (**b**) constrained.

Before carrying out the experimental modal analysis on the burner, the entire measurement chain was checked using an accelerometer calibrator and a suspended rigid block of known mass. The burner has been excited in some points using an instrumented hammer with a hard tip and measuring the dynamic response by means of accelerometers

installed with beeswax in the three orthogonal directions for each measurement point (22 measurement points). The tests have been carried out using a set of accelerometers, moving them from point to point according to the roving accelerometer method. The analysis has been performed with a bandwidth of 6400 Hz and a resolution of 0.2 Hz, averaging 4 signals. Then, the modal parameters (frequencies, damping ratios, modal vectors) have been identified using the PolyMAX algorithm, which was implemented in the software Simcenter Test Lab [41]. All signals have been acquired, recorded and processed through the software Simcenter Test Lab, version 21.2.

3. Results

3.1. Preliminary Verification of the Burner Digital Twin

The burner FE model has been preliminary verified in terms of modal frequencies, modal shapes and undamped FRF, while the modal damping ratio has been analyzed at a later stage.

3.1.1. Free-Free Configuration

In the free-free configuration, the correlation in terms of natural frequencies proved to be satisfactory, with a maximum deviation of approximately 7%, as reported in Table 1. The AUTO-MAC matrix shown in Figure 5 exhibits values concentrated along the diagonal, confirming that the experimental mode shapes were well decoupled and that no significant cross-correlation existed among the identified modes. This indicates that each mode was individually excited and correctly identified during testing, which is essential for ensuring the reliability of the modal characterization. The experimental mode shapes were visualized through the deformation of the measurement wireframe, allowing a clear interpretation of the dynamic behavior of the component. The comparison between numerical and experimental mode shapes (Figure 6) highlighted a consistent dynamic behavior, particularly for the first four modes, which exhibited the highest mass participation factors and therefore play a dominant role in the global response of the component [42]. Specifically, the first mode (a) was predominantly torsional, while the second (b) and third (c) were purely flexural, and the fourth (d) exhibited a mixed flexural–torsional character.

Starting from mode five, a noticeable increase in frequency (about 22%) was observed together with the appearance of local modes characterized by lower mass participation factors. These modes are inherently more difficult to capture and interpret in terms of global modal behavior, since their deformation is confined to limited regions of the structure, and their contribution to the overall dynamic response is marginal. As a consequence, only local modes were identified, and no significant matching between numerical and experimental mode shapes was achieved. Three representative examples of these local modes are illustrated in Figure 7. This outcome was expected, as local modes typically exhibit weaker excitation and response levels, making their experimental identification less reliable and their correlation with numerical predictions more challenging.

Globally, a good correlation of an undamped FRF spectrum has been observed. Figure 8 illustrates the "SUM FRF" spectrum, which represents the average response of all the FRFs that was taken as reference for the comparison with the numerical results. Above 2000 Hz, the quality of the experimental measurements significantly deteriorated, making the results less reliable. For this reason, data conditioning was applied by limiting the analysis frequency range to 2000 Hz. At the opposite end of the spectrum, an irregularity in the response was observed at low frequencies. This effect, which typically arises around 20–30 Hz, is directly related to the elastic cords used to suspend the burner in the free-free configuration. The cords introduce additional compliance into the system, producing artificial low-frequency modes that do not belong to the actual dynamic behavior

of the component. Since this phenomenon could strongly affect the accuracy of the modal identification, the lower bound of the frequency domain was conservatively set to 50 Hz. Highlighting this aspect is particularly important, as it underlines one of the experimental challenges of free-free testing and the need to carefully interpret low-frequency responses in suspended configurations.

Finally, to complete the pre-verification of the burner digital twin, a comparison between the experimental frequency response function (FRF) and the numerical undamped harmonic response was performed (Figure 9), using a sampling frequency of 1 Hz. The numerical response revealed the presence of an anti-mode around 1250 Hz, which did not appear in the experimental spectrum. This discrepancy can be explained by the positioning of the accelerometers, which were automatically defined by the testing software with the purpose of capturing the main global modes of the system. Anti-modes, by their nature, correspond to nodal points of vibration where the local response tends to vanish. If sensors are located close to these nodal regions, the anti-mode cannot be detected experimentally even though it exists in the numerical model. This highlights the sensitivity of experimental modal analysis to sensor placement and the importance of selecting measurement points that are representative not only of the dominant modes but also of possible anti-modes should their identification be relevant for the dynamic characterization of the component.

Table 1. Frequency comparison for free-free configuration test.

FREE-FREE CONFIGURATION			
Mode Number	**Numerical Frequency**	**Experimental Frequency**	**Relative Error**
[-]	[Hz]	[Hz]	[%]
1	914	915	0
2	973	932	4
3	1565	1455	7
4	1864	1830	2
5	2378	2288	4
6	2467	2325	6
7	2475	2378	4
8	2479	2385	4
9	2479	2441	2
10	2482	2487	0

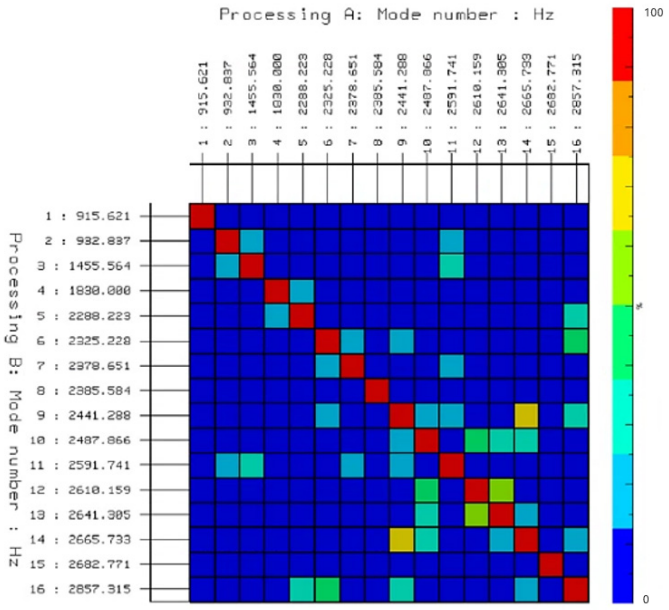
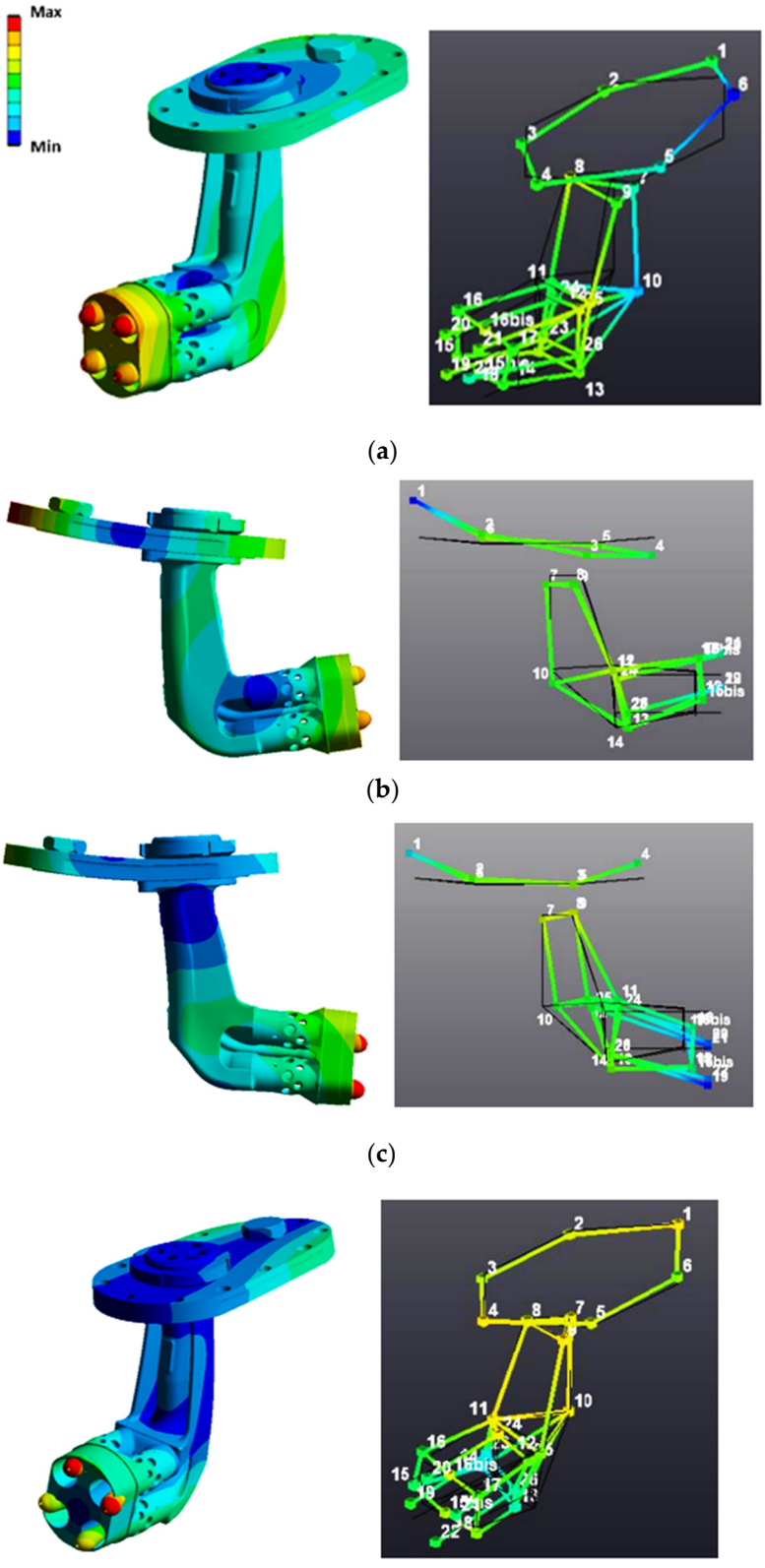


Figure 5. Auto-MAC matrix (free-free configuration).



(**a**)

(**b**)

(**c**)

(**d**)

Figure 6. Mode shapes comparison of first 4 frequencies (free-free configuration).

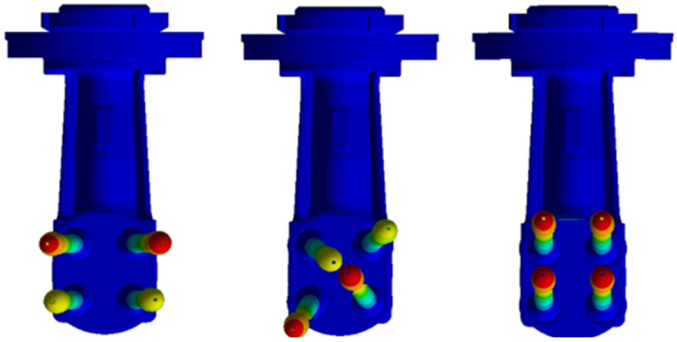


Figure 7. Local mode shapes (free-free configuration). From left side: mode 9, mode 10, mode 12.

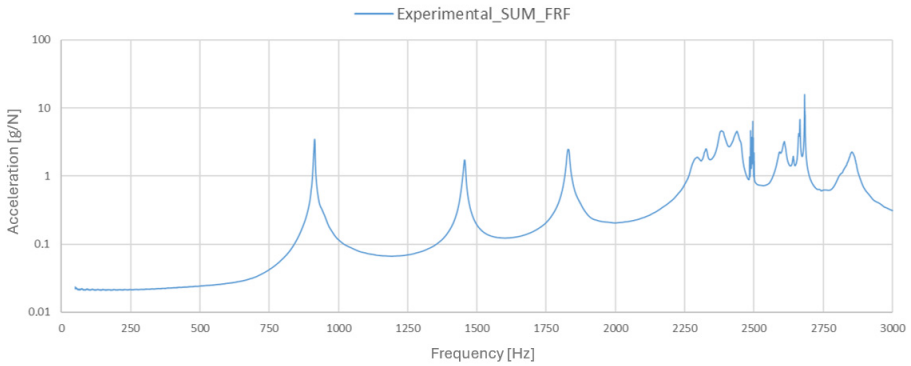


Figure 8. Sum of FRF spectrum (free-free configuration).

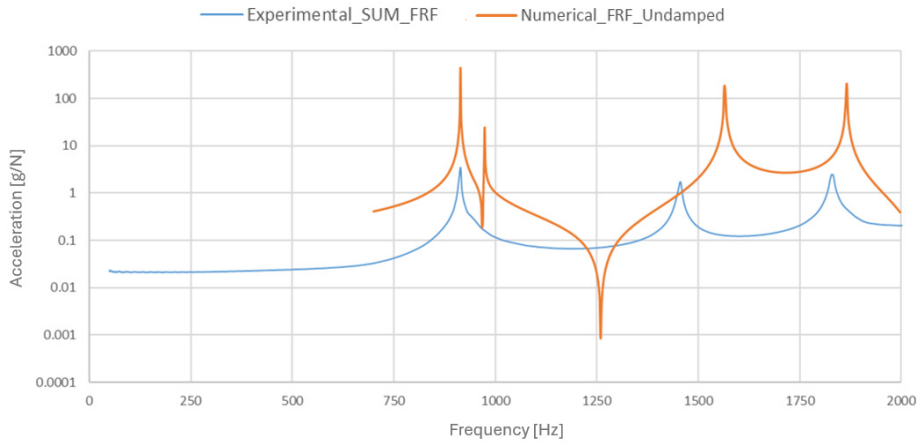


Figure 9. Undamped FRF comparison: experimental vs. numerical (free-free configuration).

3.1.2. Constrained Configuration

The same procedure adopted for the free-free configuration was applied to the constrained one. In this case, the presence of the mechanical constraint significantly influenced the results: the combustor vessel has a mass approximately three orders of magnitude greater than that of the burner, and therefore its inertia strongly affected the dynamic response of the assembled system when excited by the hammer impulse. As a consequence, the measured response included contributions not only from the burner but also from the supporting vessel. To obtain a reliable modal characterization of the burner alone, the experimental data were carefully post-processed in order to separate the mode shapes associated exclusively with the burner from those dominated by the vessel. This distinction is fundamental, since the dynamic interaction between the two components can otherwise mask or distort the burner's intrinsic modal behavior. Furthermore, in order to ensure that

numerical and experimental mode shapes were compared correctly, an evaluation of the parallelism among the corresponding eigenvectors was performed using the MAC matrix shown in Figure 10. A high degree of parallelism in the MAC indicates a strong correlation between the compared mode shapes, confirming that the filtered experimental results effectively represent the burner dynamics despite the influence of the massive vessel.

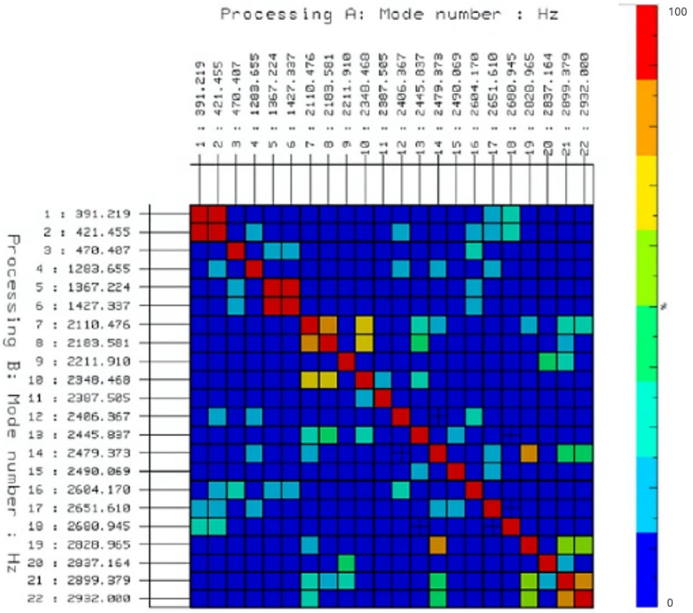
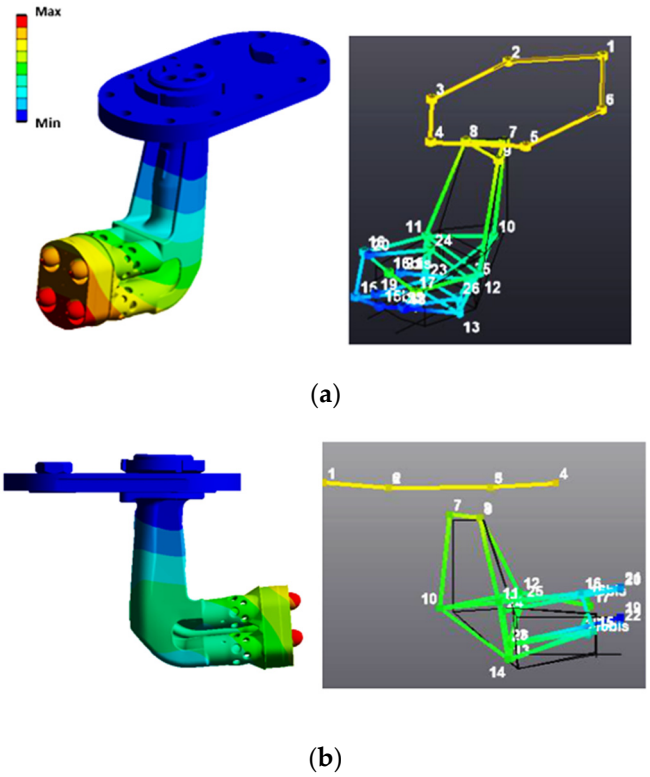


Figure 10. Auto-MAC matrix (constrained configuration).

Table 2 illustrates the mode pairs that were considered for the final comparison, which was restricted to those associated with the highest mass participation factors. The maximum frequency deviation was 7%, which is a value considered acceptable in the present context. Such tolerance is justified by the prototyping stage of the component, where the primary objective is to establish a reliable correlation between numerical predictions and experimental measurements rather than to achieve perfect numerical accuracy. In early development phases, deviations of this order are commonly tolerated, as they do not compromise the identification of the main dynamic features of the system. Moreover, in terms of mode shapes, the correlation was found to be satisfactory, as shown in Figure 11, further supporting the robustness of the adopted methodology.

Table 2. Frequency comparison for constrained configuration test.

CONSTRAINED CONFIGURATION				
Numerical Modes	**Numerical Frequency**	**Experimental Modes**	**Experimental Frequency**	**Error**
[-]	[Hz]	[-]	[Hz]	[%]
Mode 1	425	Mode 2	422	1
Mode 2	487	Mode 3	470	3
Mode 3	1315	Mode 4	1284	2
Mode 4	1463	Mode 5	1367	7
Mode 5	2240	Mode 7	2184	3
Mode 13	2905	Mode 21	2899	0



(**a**)

(**b**)

Figure 11. Mode shapes comparison for first 2 frequencies (constrained configuration): (**a**) mode 1, (**b**) mode 2.

Analysis of the FRF spectrum revealed a noticeable loss of information for frequencies above 1250 Hz. This effect is primarily associated with the introduction of the mechanical constraint, which significantly altered the system dynamics. In particular, the high mass and stiffness of the supporting combustor vessel suppressed the amplitude of the burner's response at higher frequencies, making it difficult to reliably capture the natural frequencies and mode shapes of interest. As a result, the harmonic response obtained under constrained conditions was considered insufficiently accurate for a meaningful comparison with numerical predictions. The reduction in signal clarity and the potential masking of the burner's intrinsic modes highlight the limitations of constrained testing in this context. Consequently, the free-free configuration was adopted as the reference condition for this study, as it allows the intrinsic dynamic behavior of the burner to be isolated and accurately characterized, forming a reliable basis for the subsequent steps of the methodology.

3.2. Structural Damping Estimation

The proposed procedure has been applied to the free-free configuration. Damping ratios, together with mode frequencies and mode shapes, are obtained from the ping test (see Table 3). Early-stage damping estimation in mechanical component development is important to reduce the design cycle time and directly influences high-cycle fatigue (HCF) life prediction. Excessively high damping values can lead to an underestimation of the excitations acting on the burner, resulting in non-conservative durability estimations, whereas lower values may overestimate the excitations, potentially generating a non-optimized design. The objective of this work is to define an effective method to estimate damping ratios at a prototypal stage of development, where only partial experimental data are available and typically not fully representative of the final product configuration. The procedure starts with the analysis of the experimental sum FRF spectrum. Compared to standard shaker tests [43–45], ping tests can underestimate the response amplitude, reducing the robustness of conventional damping characterization approaches such as the

widely used Rayleigh proportional damping model [46]. In this model, the damping matrix C is expressed as shown below:

$$C = \alpha M + \beta K \quad (1)$$

where M, C, and K are the system mass, damping, and stiffness matrices, and α and β are scalar parameters that can be adjusted to minimize the error between experimental and numerical damping ratios typically via least-square fitting or optimization algorithms. To improve damping accuracy at this stage, a new approach combining the Half-Power Bandwidth Method (HBM) [47] with an iterative procedure was implemented. The procedure first analyzes the frequency region around the −3 dB points of each FRF peak to determine the local variation in damping. This preliminary analysis provides an estimate of the damping range for the mode under consideration. Subsequently, an iterative tuning of the damping parameters is performed in the numerical model such that the HBM-predicted bandwidth Δf closely matches the experimental value for the first mode. Through this cycle, the numerical model reproduces the experimental response accurately even with limited data in this early prototypal phase.

Table 3. Damping ratio comparison: experimental vs. HBM.

FREE-FREE CONFIGURATION			
Mode	**Frequency**	**Experimental ξ**	**HBM ξ**
[-]	[Hz]	[%]	[%]
1	915	0.07	0.25
2	932	1.09	-
3	1455	0.25	0.35
4	1830	0.21	0.33
5	2288	0.47	-
6	2325	0.19	-
7	2378	0.37	-
8	2385	0.34	-
9	2441	0.17	-
10	2487	0	-

Damping is expressed in terms of Q (quality factor) and ξ (viscous damping ratio), whose relation is shown below:

$$Q = 1/2\,\xi \quad (2)$$

The −3 dB points define Δf, the frequency width at 67% of the reference peak amplitude, and Q can be calculated as shown below:

$$Q = f_n / \Delta f \quad (3)$$

where f_n is the natural frequency of the peak. This approach is valid for multi-degree-of-freedom systems provided that the modal peaks are well separated, as in the first, third, and fourth modes in the sum FRF spectrum (Figure 12) [47]. By combining the −3 dB analysis with the iterative HBM adjustment, the method ensures a reliable estimation of modal damping in this prototypal stage, capturing the dynamic behavior of the main modes while maintaining a practical workflow suitable for early-stage component development.

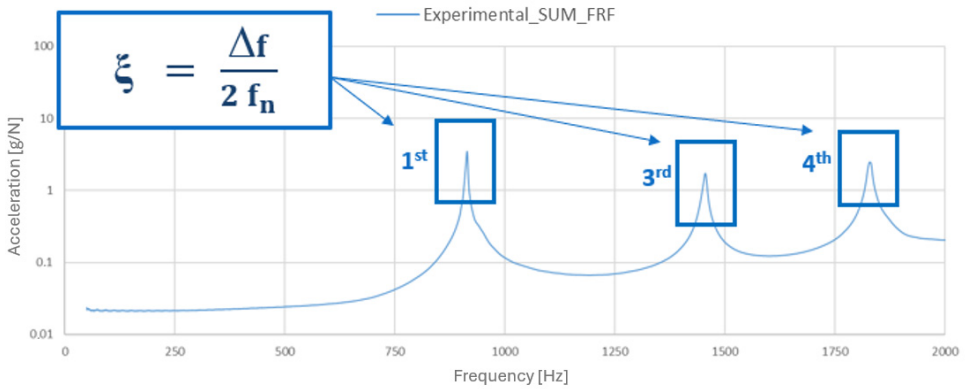


Figure 12. Damping estimation for main vibration modes.

Moreover, these modes can be approximated as single-degree-of-freedom (SDOF) systems, also considering their high mass participation factors. In this phase, the experimental data were first analyzed using the Rayleigh proportional damping model, while the values reported in the HBM column of Table 3 were obtained through the procedure involved examining the vicinity of the −3 dB points for each mode to identify a representative damping value. For each mode, three sets of damping-related values were calculated, which are summarized in Table 3 alongside the corresponding experimental damping ratios.

The mean value of damping obtained with the proposed methodology, initially estimated at 0.31% based on the analysis of the experimental FRF spectrum around the −3 dB points of the first mode (see Table 3), has been introduced in the numerical model as a constant structural damping. The FRF was then recalculated with the objective of matching the Δf evaluated at 67% of the first mode peak amplitude. Through the iterative HBM-based procedure, which fine-tunes the damping to achieve the best agreement in terms of Δf for the first mode, the final damping ratio for the burner was determined as 0.42%. Figure 13 illustrates the comparison of the response spectra obtained using the initial mean value (0.31%), the final iterative value (0.42%), and the Rayleigh model parameters (α, β), focusing on the first mode within a reduced frequency range. The graph shows that while the shape of the spectrum remains substantially unchanged with varying damping, confirming the robustness of the Δf measurement, the peak amplitude is more sensitive to the damping ratio value and varies accordingly. This result demonstrates that the iterative HBM approach effectively refines the damping estimation in this early prototypal stage, providing a reliable representation of the system's dynamic behavior.

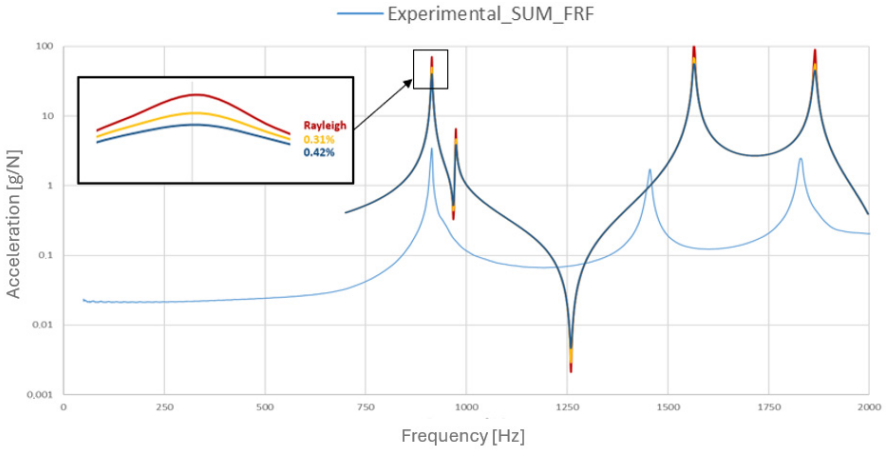


Figure 13. FRF comparison with different values of damping ratio.

4. Conclusions

Achieving future decarbonization targets in the energy production sector requires technological solutions capable of operating efficiently with low-carbon fuels. In this context, the development of hydrogen-ready gas turbines demands a rapid prototyping of dedicated gas injectors designed to operate with both natural gas and hydrogen. The design approach using additive manufacturing has been shown to offer clear advantages, including the prevention of hydrogen leaks and the ability to realize complex three-dimensional air and fuel paths in constrained spaces. A combined experimental and numerical methodology has been proposed for the estimation of structural damping in the early prototypal stage of burner development. Ping tests on the prototypal burner provided high-quality data that allowed a reliable characterization of the component dynamics even with limited available information typical of preliminary development phases. Analysis based on the standard Rayleigh proportional damping model showed limited accuracy in capturing the experimental response at this early stage. In order to improve accuracy, a novel procedure was implemented by combining the Half-Power Bandwidth Method (HBM) with an iterative approach, analyzing the frequency bandwidth around the -3 dB points of the first mode to define a representative damping value. This iterative refinement led to a final damping ratio of 0.42%, closely matching the experimental Δf and providing a robust and representative estimation of structural damping. The approach also ensured that the main dynamic behaviors were captured, while local modes with low mass participation remained difficult to detect, as expected in components with low mass and high stiffness. This methodology demonstrates that even at an early prototypal stage, reliable damping estimates can be obtained, enabling rapid convergence toward an optimal mechanical configuration and reducing the design cycle time. Future developments will focus on extending the approach to account for more pronounced nonlinear effects, such as those occurring at bolted contact interfaces, to further refine the predictive capability of the burner digital twin.

Author Contributions: Conceptualization, methodology, software and validation, A.C. and E.P.; review, A.C., E.P. and E.M. (Emanuele Matoni); supervision and project administration, E.M. (Enrico Meli), A.R. and E.P. All authors have read and agreed to the published version of the manuscript.

Funding: This research received no external funding.

Data Availability Statement: Data are unavailable due to privacy.

Acknowledgments: The authors would like to gratefully acknowledge all the colleagues from the TTL (Technology Testing Lab.), MPE (Material and Process Engineering) and CBT (Gas Turbine Combustion) design teams of Nuovo Pignone Tecnologie s.r.l., part of Baker Hughes company, for their contribution to this work and their support during the whole research activity.

Conflicts of Interest: Authors Egidio Pucci and Emanuele Matoni were employed by the company Baker Hughes, Nuovo Pignone Tecnologie. The remaining authors declare that the research was conducted in the absence of any commercial or financial relationships that could be construed as a potential conflict of interest.

References

1. Clean Hydrogen Joint Undertaking. *Strategic Research and Innovation Agenda 2021–2027*; Publications Office: Luxembourg, 2022.
2. Fuel Cells and Hydrogen Joint Undertaking. *Hydrogen Roadmap Europe: A Sustainable Pathway for the European Energy Transition*; Publications Office: Luxembourg, 2019. [CrossRef]
3. IEA. *The Future of Hydrogen*; International Energy Agency: Paris, France, 2019.
4. ETN Global. *The Path Towards a Zero-Carbon Gas Turbine*; ETN Global: Brussels, Belgium, 2020.
5. Cocchi, S.; Provenzale, M.; Cinti, V.; Carrai, L.; Sigali, S.; Cappetti, D. Experimental Characterization of a Hydrogen Fuelled Combustor with Reduced NOx Emissions for a 10 MW Class Gas Turbine. In Proceedings of the ASME Turbo Expo 2008: Power for Land, Sea, and Air, Berlin, Germany, 9–13 June 2008; Volume 3, pp. 991–1000. [CrossRef]

6. Cerutti, M.; Pucci, E.; Romano, C.; Dabiru, V.R. Development of an Hydrogen Fueled Gas Turbine Combustion System From Conceptual Through Full Scale Verification Test. In Proceedings of the ASME Turbo Expo 2023: GT2023-102502, Boston, MA, USA, 26–30 June 2023.
7. Noble, D.R.; Zhang, Q.; Shareef, A.; Toothle, J.; Meyers, A.; Lieuwen, T. Syngas Mixture Composition Effects Upon Flashback and Blowout. In Proceedings of the ASME Turbo Expo 2006: Power for Land, Sea, and Air, Barcelona, Spain, 8–11 May 2006; Volume 1, pp. 357–368. [CrossRef]
8. Marek, J.C.; Smith, T.D.; Kundu, K. Low Emission Hydrogen Combustors for Gas Turbines Using Lean Direct Injection. In Proceedings of the 41st IAA/ASME/SAE/ASEE Joint Propulsion Conference and Exhibit, Tucson, AZ, USA, 13 July 2005; ASME. Available online: https://ntrs.nasa.gov/citations/20080002274 (accessed on 26 November 2025).
9. Dodo, S.; Asai, T.; Koizumi, H.; Yoshida, S.; Inoue, H. Combustion Characteristics of a Multiple-Injection Combustor for Dry Low-NOx Combustion of Hydrogen-rich Fuels Under Medium Pressure. In Proceedings of the ASME 2011 Turbo Expo: Turbine Technical Conference and Exposition, Vancouver, BC, Canada, 6–10 June 2011; Volume 2, p. 467. [CrossRef]
10. Funke, H.H.W.; Boerner, S.; Keinz, J. Experimental and Numerical Characterization of the Dry Low NOx Micromix Hydrogen Combustion Principle at Increased Energy Density for Industrial Hydrogen Gas Turbine Application. In Proceedings of the ASME Turbo Expo 2013: Turbine Technical Conference and Exposition, San Antonio, TX, USA, 3–7 June 2013; Volume 1. [CrossRef]
11. Cerutti, M.; Giannini, N.; Ceccherini, G.; Meloni, R.; Matoni, E.; Romano, C.; Riccio, G. Dry Low NOx Emissions Operability Enhancement of a Heavy-Duty Gas Turbine by Means of Fuel Burner Design Development and Testing. In Proceedings of the ASME Turbo Expo 2018: Turbomachinery Technical Conference and Exposition, Oslo, Norway, 11–15 June 2018; Volume 4.
12. Cerutti, M.; Cocchi, S.; Modi, R.; Sigali, S.; Bruti, G. Hydrogen Fueled Dry Low NOx Gas Turbine Combustor Conceptual Design. In Proceedings of the ASME Turbo Expo 2014: Turbine Technical Conference and Exposition, Düsseldorf, Germany, 16–20 June 2014; Volume 4.
13. Meloni, R.; Cerutti, M.; Zucca, A.; Mazzoni, M. Numerical Modelling of NOx Emissions and Flame Stabilization Mechanisms in Gas Turbine Burners Operating with Hydrogen and Hydrogen-Methane Blends. In Proceedings of the ASME Turbo Expo 2020: Turbomachinery Technical Conference and Exposition, Online, 21–25 September 2020; Volume 4. [CrossRef]
14. Zajadatz, M.; Güthe, F.; Freitag, E.; Ferreira-Providakis, T.; Wind, T.; Magni, F.; Goldmeer, J. Extended Range of Fuel Capability for GT13E2 AEV Burner With Liquid and Gaseous Fuels. *J. Eng. Gas Turbines Power* **2019**, *141*, 051017. [CrossRef]
15. Meloni, R.; Babazzi, G.; Giannini, N.; Castellani, S.; Nassini, P.C.; Galeotti, S.; Picchi, S.; Becchi, R.; Andreini, A. Thickened Flame Model Extention For Dual Gas GT Combustion: Validation Against Single Cup Atmospheric Test. In Proceedings of the ASME 2024 Turbo Expo: Turbine Technical Conference and Exposition, London, UK, 24–28 June 2024; GT2024-122234.
16. Ansari, N.; Orsino, S.; Meloni, R.; Pucci, E.; Castellani, S.; Andreini, A.; Valera-Medina, A. Large-Eddy Simulation of a Non-Premixed Ammonia-Hydrogen Flame: NOx emission and Flame Characteristics Validation. In Proceedings of the ASME 2024 Turbo Expo: Turbine Technical Conference and Exposition, London, UK, 24–28 June 2024; GT2024-129248.
17. Sullivan-Lewis, E.; McDonell, V. Flameholding Tendencies of Natural Gas and Hydrogen Flames at Gas Turbine Premixer Conditions. In Proceedings of the ASME Turbo Expo 2014: Turbine Technical Conference and Exposition, Dusseldorf, Germany, 16–20 June 2014; Volume 4.
18. Baldini, M.; Carta, R.; Cerutti, M.; Pucci, E.; Grosso, M.; Romano, C.; Sarti, G. NovaLTTM16 H_2 Gas Turbine test campaign up to 100% H2. In Proceedings of the Gastech 2024 Technical Conference and Exposition, Houston, TX, USA, 17–20 September 2024.
19. Blakey-Milner, B.; Gradl, P.; Snedden, G.; Brooks, M.; Pitot, J.; Lopez, E.; Leary, M.; Berto, F.; Plessis, A.D. Metal additive manufacturing in aerospace: A review. *Mater. Des.* **2021**, *209*, 110008. [CrossRef]
20. Najmon, J.; Raeisi, S.; Tovar, A. Review of additive manufacturing technologies and applications in the aerospace industry. *Addit. Manuf. Aerosp. Ind.* **2019**, *209*, 7–31. [CrossRef]
21. Chowdhury, S.; Yadaiah, N.; Prakash, C.; Ramakrishna, S.; Dixit, S.; Gupta, L.R.; Buddhi, D. Laser powder bed fusion: A state-of-the-art review of the technology, materials, properties & defects, and numerical modelling. *J. Mater. Res. Technol.* **2022**, *20*, 2109–2172. [CrossRef]
22. Ahn, D.G. Directed Energy Deposition (DED) Process: State of the Art. *Int. J. Precis. Eng. Manuf.-Green Tech.* **2021**, *8*, 703–742. [CrossRef]
23. Murugan, P.D.; Vijayananth, S.; Natarajan, M.P.; Jayabalakrishnan, D.; Arul, K.; Jayaseelan, V.; Elanchezhian, J. A current state of metal additive manufacturing methods: Review. *Mater. Today Proc.* **2022**, *59*, 1277–1283. [CrossRef]
24. Orme, M.E.; Gschweitl, M.; Ferrari, M.; Vernon, R.; Madera, I.J.; Yancey, R.; Mouriaux, F. Additive manufacturing of lightweight, optimized, metallic components suitable for space flight. *J. Spacecr. Rocket.* **2017**, *54*, 1050–1059. [CrossRef]
25. Caujolle, M. First Titanium 3D-Printed Part Installed into Serial Productionaircraft. 2017. Available online: https://www.airbus.com/en/newsroom/press-releases/2017-09-first-titanium-3d-printed-part-installed-into-serial-production#related-assets (accessed on 26 November 2025).
26. Bandini, A.; Cascino, A.; Meli, E.; Pinelli, L.; Marconcini, M. Improving Aeromechanical Performance of Compressor Rotor Blisk with Topology Optimization. *Energies* **2024**, *17*, 1883. [CrossRef]

27. Allison, T.; Rimple, A.; Pelton, R.; Moore, J.; Wilkes, J.; Wygant, K. Manufacturing and testing experience with direct metal laser sintering for closed centrifugal compressor impellers. *Turbomach. Pump Symp.* **2014**. [CrossRef]
28. Jia, D.; Li, F.; Zhang, Y. 3D-printing process design of lattice compressor impeller based on residual stress and deformation. *Sci. Rep.* **2020**, *10*, 600. [CrossRef]
29. Saltzman, D.; Bichnevicius, M.; Lynch, S.; Simpson, T.W.; Reutzel, E.W.; Dickman, C.; Martukanitz, R. Design and evaluation of an additively manufactured aircraft heat exchanger. *Appl. Therm. Eng.* **2018**, *138*, 254–263. [CrossRef]
30. Jafari, D.; Wits, W.W. The utilization of selective laser melting technology on heat transfer devices for thermal energy conversion applications: A review. *Renew. Sustain. Energy Rev.* **2018**, *91*, 420–442. [CrossRef]
31. Wang, Z.; Wang, J.; Lin, X.; Kang, N.; Zhang, T.; Wang, Y.; Wang, L.; Dang, C.; Huang, W. Solidification microstructure evolution and its correlations with mechanical properties and damping capacities of Mg-Al-based alloy fabricated using wire and arc additive manufacturing. *J. Mater. Sci. Technol.* **2022**, *144*, 28–44. [CrossRef]
32. Gibson, I.; Rosen, D.; Stucker, B.; Khorasani, M. *Additive Manufacturing Technologies*, 3rd ed.; Springer: Berlin/Heidelberg, Germany, 2021.
33. Diegel, O.; Nordin, A.; Motte, D. *A Practical Guide to Design for Additive Manufacturing*; Springer: Berlin/Heidelberg, Germany, 2020.
34. Pastor, M.; Binda, M.; Harčarik, T. Modal Assurance Criterion. *Procedia Eng.* **2012**, *48*, 543–548. [CrossRef]
35. Proso, U.; Slavič, J.; Boltežar, M. Vibration-fatigue damage accumulation for structural dynamics with non-linearities. *Int. J. Mech. Sci.* **2016**, *106*, 72–77. [CrossRef]
36. Piraccini, M.; Di Sante, R. Measurement of nonlinear vibration response in aerospace composite blades using pulsed airflow excitation. *Measurement* **2018**, *130*, 422–434. [CrossRef]
37. Lozia, Z.; Zdanowicz, P. Simulation assessment of the half-power bandwidth method in testing shock absorbers. *Open Eng.* **2021**, *11*, 120–129. [CrossRef]
38. Papagiannopoulos, G.A.; Hatzigeorgiou, G.D. On the use of the half-power bandwidth method to estimate damping in building structures. *Soil Dyn. Earthq. Eng.* **2011**, *31*, 1075–1079. [CrossRef]
39. Wu, B.S. A correction of the half-power bandwidth method for estimating damping. *Arch. Appl. Mech.* **2014**, *85*, 315–320. [CrossRef]
40. Simcenter Testlab Software. Available online: https://plm.sw.siemens.com/it-IT/simcenter/physical-testing/testlab/ (accessed on 26 November 2025).
41. Irvine, T. Effective Modal Mass and Modal Participation Factors. 2013. Available online: http://www.vibrationdata.com/tutorials2/ModalMass.pdf (accessed on 26 November 2025).
42. Waters, T. Vibration testing. In *Fundamentals of Sound and Vibration*; CRC Press: Boca Raton, FL, USA, 2015; pp. 469–508.
43. Peeters, B.; Van Der Linden, P.; De Veuster, C. Performance of miniature shakers for vehicle component testing. In Proceedings of the IMAC, Dearborn, MI, USA, 19–22 January 2004; Volume 22.
44. Peres, M.A.; Bono, R.W.; Avitabile, P. Effects of shaker, stinger and transducer mounting on measured frequency response functions. In Proceedings of the ISMA 2012 International Conference on Noise and Vibration Engineering, Leuven, Belgium, 17–19 September 2012; pp. 1475–1489.
45. Liu, M.; Gorman, D.G. Formulation of Rayleigh damping and its extensions. *Comput. Struct.* **1995**, *57*, 277–285. [CrossRef]
46. Sun, P.; Wang, D. Comparison of damping parameters based on the half-power bandwidth methods of viscous and hysteretic damping models. *J. Vib. Control* **2021**, *29*, 968–979. [CrossRef]
47. Irvine, T. The half power bandwidth method for damping calculation. *Vibrationdata* **2005**, 1–8. Available online: https://www.vibrationdata.com/tutorials2/half_power_bandwidth.pdf (accessed on 26 November 2025).

Disclaimer/Publisher's Note: The statements, opinions and data contained in all publications are solely those of the individual author(s) and contributor(s) and not of MDPI and/or the editor(s). MDPI and/or the editor(s) disclaim responsibility for any injury to people or property resulting from any ideas, methods, instructions or products referred to in the content.